MATERIALS CHEMISTRY FRONTIERS

RESEARCH ARTICLE

View Article Online
View Journal | View Issue

Cite this: *Mater. Chem. Front.*, 2026, **10**, 1418

Diazadioxa[8]circulene – a platform for stable antiaromatic radicals with strong NIR absorption

Cecilia Bruschi, †[ab] Ihor Sahalianov, †[ab] Yuri Tanuma,[a] Levani Skhirtladze,[a] Rashid Valiev,[c] Xinyi Cai,[d] Feng Gao,[d] Mikhail Vagin,[ab] Yann Lie,[e] Michael Pittelkow,[e] Renee Kroon *[ab] and Glib Baryshnikov *[ab]

Received 26th January 2026,
Accepted 12th February 2026

DOI: 10.1039/d6qm00054a

rsc.li/frontiers-materials

Stable organic radicals exhibiting absorption capabilities in the visible and near-infrared regions (NIR) are appealing candidates for a wide range of applications, including photovoltaics, photothermal applications, anticounterfeiting and information encryption/decryption. Hetero[8]circulenes represent a promising π-extended platform for stable delocalized radicals with rich possibilities for chemical tuning. In this paper, we present the stable cation radical of diazadioxa[8]circulene with reduced symmetry showing a sharp and strong peak ($\varepsilon \sim 2 \times 10^4$ M^{-1} cm^{-1}) in the NIR at 939 nm. The diazadioxa[8]circulene cation radical can be obtained *via* chemical doping using Magic Blue, or *via* electrochemical doping. It remains stable for several days without any significant change in the absorption spectra. Furthermore, according to magnetic criteria of aromaticity, it exhibits antiaromatic behaviour. Advanced theoretical calculations predict NIR emission for the radical cation through an anti-Kasha $D_4 \rightarrow D_0$ transition, which is experimentally not detectable due to non-radiative deactivation pathways. Our RI-CC2 theoretical calculations also corroborate the blue emission of neutral circulene from the bright lowest singlet excited state S_1, which was previously unexplained due to TD-DFT artefact predicting the dark S_1 state. These results open the opportunities for the practical application of diazadioxa[8]circulene cation radicals in photovoltaics, sensors and photothermal imaging.

Introduction

Hetero[8]circulenes (H8Cs) represent a class of polyaromatic π-conjugated organic compounds with a central eight-membered ring surrounded by eight arene (benzene, naphthalene, anthracene, *etc.*) or hetarene (pyrrole, thiophene, furan, *etc.*) moieties.[1–3] The appealing features of H8Cs are their high symmetry (up to D_{8h} space point group), planarity, double aromaticity and high stability. Therefore, H8Cs have been explored in OLEDs as blue-emissive materials,[4–6] in field effect transistors as the charge-carrier transporting materials,[7–9] and as building blocks for two-dimensional covalent and metal–organic frameworks.[10–12] In addition, H8Cs are characterized by extended π-delocalization, potentially enabling a platform for stable radicals with strongly delocalised unpaired electrons.

This design strategy for stable radicals – an alternative to atom-centred luminescent radicals with sterically protected unpaired electrons – has already been described for other organic compounds.[13–17] For example, Chen *et al.* reported bisphenalenyl radicals (Fig. 1) exhibiting anti-Kasha emissions, while the D_1 excited state is non-emissive due to its small energy difference (ΔE) with the ground state ($\Delta E \sim 1$ eV).[18,19] Thanks to the efficient delocalization of the unpaired electron over the bisphenalenyl core, these radicals show an excellent photostability with a half-life ($t_{1/2}$) of 9.5×10^4 s under 350 nm irradiation. Yamaguchi *et al.* synthesized planar boron-containing triphenylmethyl radicals (B-TPM, Fig. 1), which demonstrated red fluorescence from the D_1 state, in agreement with the Kasha rule.[20] These radicals show high chemical stability at room temperature. Another example of a stable, delocalized luminescent radical is the carbazole/carbonyl hybridized luminophore TBIQ reported by Lee *et al.*, which showed strong orange emission ($\lambda_{em} \sim 600$ nm) and additionally a white emission when mixed with the neutral blue-emissive TBIQ.[21]

In the context of H8Cs, tetraoxa[8]circulenes (TOCs)[22] and tetrabenzotetraaza[8]circulene (TB-TAC)[23] were shown to produce stable cation radicals when doped with strong oxidants

[a] *Department of Science and Technology, Laboratory of Organic Electronics, Linköping University, SE-60174 Norrköping, Sweden. E-mail: glib.baryshnikov@liu.se*
[b] *Wallenberg Initiative Materials Science for Sustainability, Department of Science and Technology, Linköping University, SE-60174 Norrköping, Sweden*
[c] *Department of Chemistry, Faculty of Science, University of Helsinki, P. O. Box 55 (A. I. Virtanens plats 1), Finland*
[d] *Department of Physics, Chemistry and Biology (IFM), Linköping University, SE-581 83 Linköping, Sweden*
[e] *Department of Chemistry, University of Copenhagen, Universitetsparken 5, Copenhagen Ø, DK-2100, Denmark*
† These authors contributed equally to this work.

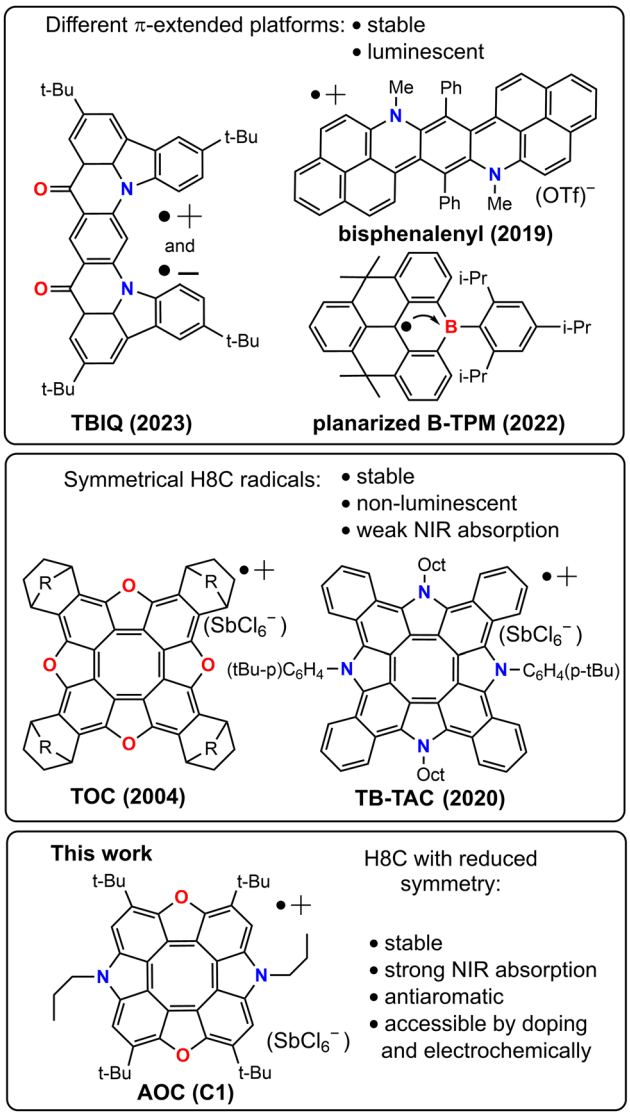

Fig. 1 Examples of the reported π-delocalized radicals based on different platforms including H8Cs (R = $-CH_2-$ and $-(CH_2)_2-$ for TOC) and the peculiarities of the newly synthesized cation radical of AOC (**C1**) presented in this paper.

such as [$NAP^{+\bullet}$ $SbCl_6^-$] and tris(4-bromophenyl)ammoniumyl hexachloroantimonate (Magic Blue), respectively. However, the optical properties of TOCs and TB-TAC radicals (Fig. 1), and especially their luminescence, do not show the distinct features typically associated with the presence of unpaired electrons. Indeed, TOC radicals exhibit a red-shifted absorption in the visible region compared to their neutral form and the appearance of new weak bands in the 600–800 nm region, but they do not show any detectable emission.[22] Similarly, TB-TAC radicals present absorption bands in the visible region at 486 and 605 nm, but no luminescence was observed for these radicals.[23] Both TB-TAC and TOC radicals exhibit featureless and broad absorption in the near-infrared region (1000–2000 nm[23] and 800–1100 nm,[22] respectively), which are associated with the number of low-lying and doublet excited states with small oscillator strengths.[23] However, due to the high symmetry of the TB-TAC and TOC units (D_{4h} symmetry point group) there are several symmetry-forbidden electronic transitions and thus they are not observed in the absorption and emission spectra. Additionally, the number of low-lying doublet excited states in the spectrum of the TB-TAC cation radical manifested as a continuous 1000–2000 nm absorption band prevents the observation of fluorescence due to dominating non-radiative quenching in the near-infrared region (NIR).

In this work, we overcome the challenges associated with symmetry-forbidden transitions and tetrabenzoannelation-assisted red-shifted absorption/emission by using non-benzoannelated diazadioxa[8]circulene (AOC, referred to as **C1** in the text) as the precursor for cation radicals.[1] **C1** also exhibits a reduced symmetry (D_{2h} symmetry point group) compared to TOC and TAC chromophores. Through redox doping with Magic Blue, we were able to obtain a cation radical of **C1**, which showed an extraordinary intense absorption in the near-infrared region at 939 nm. The isolated radical compound also exhibits good stability (at least two days in dichloromethane solution and four days in a poly(methyl methacrylate) (PMMA) film without significant changes in the vis-NIR absorption spectra). Based on the detailed quantum-chemical calculations, we assigned the strong NIR absorption to the D_0–D_4 electronic transition. We believe that shifting this band into the blue region, together with confining the radical within the rigid matrix, will enable the observation of the radical fluorescence *via* the anti-Kasha mechanism, *i.e.* asymmetrical heterocirculenes represent a promising platform for the new class of stable luminescent radicals. We also addressed the computational challenge related to the photophysical behaviour of neutral TAC chromophores, which show a bright blue fluorescence recorded experimentally, but not predicted through density functional theory (DFT) calculations. Lastly, we have also characterized the aromaticity of **C1** and of its corresponding cation radical (**R1**). We have found that neutral **C1** demonstrates the typical "bifacial" aromaticity of H8Cs (inner cyclooctatetraene core sustains strong paratropic magnetically induced ring current associated with antiaromatic behaviour and outer perimeter exhibits strong diatropic ring current corresponding to aromatic character), while the cation radical demonstrates the double paratropicity (antiaromaticity) within inner and outer conjugation circuits. This is a new example of stable antiaromatic systems that opens new possibilities for probing the effects of an antiaromatic environment on the electronic structure and reactivity of molecular systems.

Results and discussion

Synthesis and characterization of the circulene radical cation

Diazadioxa[8]circulene[1] **C1** was oxidized using tris(4-bromophenyl)ammoniumyl hexachloroantimonate (Magic Blue), a well-known effective one-electron oxidant, to produce the circulene radical cation **R1** (Fig. 2c).[24,25] To optimize the molar ratio of the redox reaction, a titration of the circulene **C1** in dichloromethane (DCM) was carried out by the slow addition of a Magic Blue solution (Fig. 2a) in DCM. Upon the addition of Magic Blue

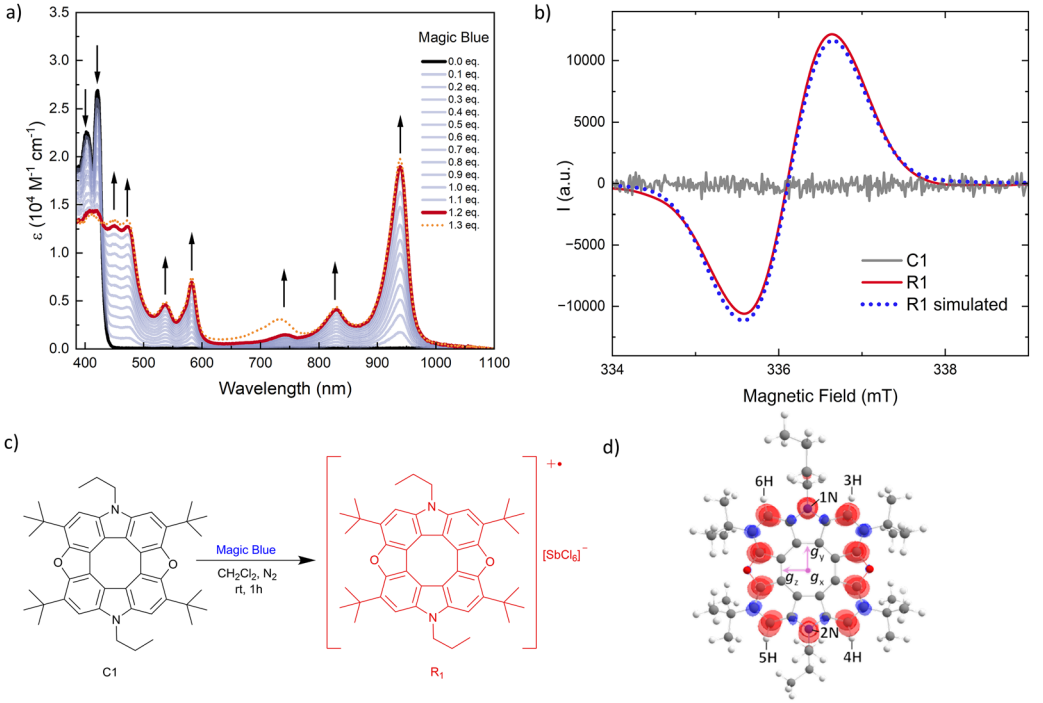

Fig. 2 (a) Absorption spectra evolution of circulene **C1** upon titration with Magic Blue, in dichloromethane. (b) Room temperature EPR spectra of a dichloromethane solution of the circulene **C1** and of the corresponding radical cation **R1**. (c) Synthesis of the radical cation by the oxidation of the diazadioxa[8]circulene **C1** with Magic Blue. (d) Spin distribution on radical cation **R1**. Red and blue bubble plots show positive and negative signed spin distribution (spin α–spin β). Isosurface cut-off is set at 0.002 e a_0^{-3}.

to the **C1** solution, the peak maxima of the starting material **C1** at 402 and 420 nm decreased while several new peaks appeared in the visible spectrum (λ_{max} = 450, 473, 537 and 582 nm), resulting in a solution colour change from yellow to red. Furthermore, new peaks were identified in the NIR region: two broad peaks at 743 and 829 nm and a sharp peak at 939 nm. It is noteworthy that the longest wavelength peak (939 nm) is also the strongest, with a remarkable high molar extinction coefficient (ε) of $\sim 2 \times 10^4$ M^{-1} cm^{-1}. This value also exceeds those of the product peaks in the visible region. Saturation of the spectrum is reached after the addition of 1.2 equivalents of Magic Blue, suggesting an equimolar ratio for the two reactants. The slight imbalance of the stoichiometry can be explained by the low solution concentrations used, which are more susceptible to deviations. Continued titration of **C1** with Magic Blue (1.3 equivalents) results in the emergence of a new peak at 732 nm, which can be attributed to the Magic Blue in excess (see Fig. S4 for the absorption spectrum of Magic Blue in dichloromethane). Subsequently, a larger scale reaction (30 mg) was carried out under a N_2 atmosphere by adding Magic Blue in a $\sim$1 : 1 ratio to an anhydrous dichloromethane solution of the circulene **C1**. After stirring for one hour at room temperature, the product **R1** was purified the by the addition of an excess of *n*-hexane to a concentrated dichloromethane solution of the reaction mixture to remove excess **C1** and byproduct tris(4-bromophenyl)amine (t-BPA, Fig. S1), and isolated as an amorphous red powder with a yield of 84%. The absorption spectrum of the isolated product was recorded (Fig. S5). The ratio of the visible region peak (around 411 nm) to the NIR peak (around 939 nm), which is attributable only to the product, represents a sound parameter for evaluating product purity from optical spectroscopy analysis, since the starting material and the product overlap in the visible region. Therefore, we compared the ratio obtained from the absorption spectrum of excess of Magic Blue (1.3 equivalents) added to **C1** (Fig. 2a), which we assume to be completely converted to **R1**, with the ratio obtained from the absorption spectrum of the product isolated after the larger-scale reaction (Fig. S5). The difference between the two ratios remains lower than 6%. This falls within the experimental margin of error, allowing us to assume the starting material to be present in negligible amounts. Furthermore, the low absorption recorded between 600 nm and 720 nm, where the Magic Blue absorbs, allows us to assume the absence of the oxidant.

A comparison between the FTIR spectra of the starting materials and the product (Fig. S2) further corroborated the optical spectroscopy results. Indeed, the peaks of the Magic Blue at 3079 and 3051 cm^{-1}, that are attributed to the C–H stretching of the tris(4-bromophenyl)ammoniumyl moiety, are absent in the spectra of the circulene radical cation **R1**. A detailed description and interpretation of the FTIR peaks of the circulene **C1** was previously published[26] and a similar explanation can be applied to the peaks of the product **R1**. The compound is quite stable in solution. Indeed, only a gradual reformation of the neutral circulene **C1** was observed after two days, as indicated by the appearance and intensification of its peaks at 402 and 420 nm (see Fig. S7). Furthermore, the compound also exhibits good

stability in its solid state. No significant changes were observed in the absorption spectra of a radical film in a PMMA matrix (1.0% w/w), even after four days (Fig. S8).

Continuous wave (CW) X-band electron paramagnetic resonance (EPR) measurements were performed to prove the presence of an unpaired electron in the electronic configuration of the circulene radical cation **R1**. As expected, no EPR peaks were detected for dichloromethane solutions of the neutral circulene **C1** (Fig. 2b). Conversely, EPR analysis of dichloromethane solutions of **R1** confirmed the presence of radicals, as evidenced by the observed broad peak (Fig. 2b). Note that the position of this peak was different from the one recorded for the unpaired electron of Magic Blue (Fig. S3). Considering the presence of nitrogen atoms and the spin density positioned on them (see below), the EPR spectrum is expected to show 25 spikes, which consist of 5 from the two equivalent nitrogen nuclei, multiplied by 5 from the four equivalent hydrogen atoms. However, in the solution sample, the spin–spin relaxation time (T_2) is shortened by intensive interactions with neighbouring nuclei. The shortening of T_2 causes line broadening of EPR spectra. Curve-fitting of the experimental spectrum is performed as a spin system of two equivalent nitrogen and four equivalent hydrogen atoms, as the spin density is mainly delocalised throughout the circulene core. The derived EPR parameters are summarised in Table S1. The fitting calculated *g*-factor of the peak was determined to be 2.0079, which is a typical value for organic molecules and is in the range of reported values for similar aza[8]circulene molecules.[23,27] The broad peak is Voigt-lineshape, which is a convolution of Gaussian- and Lorentzian-lineshape (Table S1). The dominant Gaussian-type component suggests that the broadening is mainly due to unresolved hyperfine structure, while the Lorentzian component is attributed to the T_2 relaxation by collision.[28]

The DFT calculations on the radical cation **R1** show that the spin density is delocalised throughout the outer ring of the circulene molecular framework (Fig. 2d). Calculated *g*-factor is $g_x = 2.0017$, $g_y = 2.0029$, $g_z = 2.0033$, and $g_{iso} = 2.0026$, which are typical for organic molecules. The difference from the experimental value is mainly attributed to the contribution from the $SbCl_6^-$ and byproduct (Fig. S1) present in the solution, which are not considered in the DFT calculations. Hyperfine coupling tensors (A) are also calculated for nitrogen and hydrogen atoms in the central circulene molecular framework, where the spin density lies on/near them, and are summarised in Table S2. The two nitrogen atoms possess axial A values of $A_x^N \approx 23.2$ MHz, $A_y^N \approx 1.0$ MHz, $A_z^N \approx 1.1$ MHz, and $A_{iso}^N \approx 8.5$ MHz and the hydrogen atoms possess $A_x^H \approx -10.4$ MHz, $A_y^H \approx -3.9$ MHz, $A_z^H \approx -14.4$ MHz, and $A_{iso}^H \approx 9.6$ MHz. Considering the averaging of anisotropy in the solution sample, these results are consistent with the experimentally obtained values.

To verify if we could experimentally detect the NIR emission predicted by calculations, we performed photoluminescence characterization of radical **R1**. However, no emission was observed for the radical in dichloromethane solution (298 K). Therefore, we tested the emission of a film of **R1** in PMMA matrix (1.0% w/w), because the PMMA matrix combines optical transparency with a more rigid environment for the radical cation **R1** that potentially reduces non-radiative decay pathways. Despite the use of a rigid matrix, an unreproducible emission at 977 nm was obtained when irradiating the radical film with an 850 nm continuous-wave (CW) laser diode.

Single-crystal electron diffraction

To further prove the formation of the radical cation **R1**, single-crystal electron diffraction (ED) measurements were performed. Slow evaporation of a saturated solution of **R1** in CH_2Cl_2/*n*-heptane afforded red microcrystals suitable for this analysis. The crystal structure is shown in Fig. 3a and it confirms the formation of radical cations. The radical cation **R1** crystallizes in the triclinic $P\bar{1}$ space group. The asymmetric unit consists of one half of a circulene unit and one half of an $SbCl_6^-$ counterion. Bond lengths corresponding to the formally double bonds are systematically shorter than those in the previously reported single-crystal structure of **C1**[1] (CCDC: 945393, see the SI, Fig. S9), consistent with previous observations on persistent circulene radical cations.[23] The bond length alternation (BLA, defined as the difference between the average formal single and double bonds in a π-conjugated system) is seemingly higher in **R1** than in **C1**. This

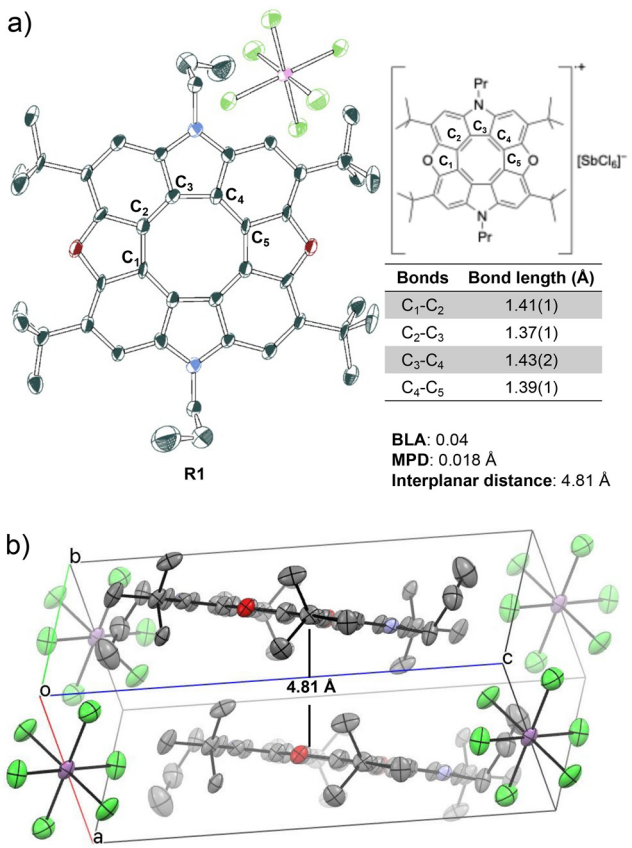

Fig. 3 (a) SC-ED structure of **R1** represented as ORTEP diagrams the 50% thermal ellipsoids. Non-hydrogen atoms are represented as 50% probability thermal ellipsoids, and selected bond lengths are given in Å (uncertainty in brackets). Atoms are colored grey (carbon), red (oxygen), and blue (nitrogen). Hydrogens are omitted for clarity. (b) Packing diagram of **R1**, the interplanar distance between the residues is shown.

increase may indicate enhanced antiaromatic character in **R1**, although the magnitude of the difference is small and should be interpreted cautiously given the experimental uncertainties. The mean planar deviation (MPD) of **R1** (MPD = 0.018 Å) is comparable to the neutral **C1** (MPD = 0.012 Å), indicating that both circulenes adopt a nearly planar conformation. The packing diagram (Fig. 3b) shows two closest radical cations separated by an interplanar distance of 4.81 Å. This notably larger separation compared to the 2.923 Å between neutral **C1** residues can be attributed to Coulombic repulsion between the positively charged radical species in the lattice.

Cyclic voltammetry and spectroelectrochemistry

Electrochemical characterisation and the *in situ* spectroelectrochemistry characterisation of the circulene **C1** were performed to produce the radical cation both chemically and electrochemically, and to compare the results of the two methods. A cyclic voltammetry (CV) of the circulene **C1** was first carried out to evaluate the potential necessary for the formation of the radical cation. The CV was performed in dichloromethane using tetrabutylammonium hexafluorophosphate ($TBAPF_6$) as the supporting electrolyte and ferrocene/ferrocenium couple (Fc/Fc^+) as internal standard (Fig. 4a). The first oxidation potential was recorded at 0.54 V. We attribute this quasi-reversible process to the radical cation formation. A secondary irreversible peak, related to the dication production, was observed at a higher potential of 1.09 V. Since the reduction potential of Magic Blue is 0.7 V,[29] it follows that the formation of the radical cation **R1** by electron transfer with Magic Blue is thermodynamically favoured, whereas the driving force for the formation of the di-cation is insufficiently high.

Following the measurements of the oxidation potentials of the circulene **C1**, *in situ* spectroelectrochemistry characterisation was performed to monitor the optical evolution of the radical cation electrochemical production. The spectroelectrochemical analysis was conducted in dichloromethane solution (0.1 M $TBAPF_6$), using a Pt honeycomb electrode. Upon application of a potential of ~0.6 V (the first oxidation potential of **C1**), an optical spectrum was obtained, which exhibited a resemblance to the spectrum of the redox reaction product **R1** (Fig. 4b). Over time, the intensity of the spectrum increased, reaching a plateau after almost 30 seconds. This result confirms that the isolated product formed by reacting circulene **C1** and Magic Blue is the radical cation **R1**, and that the chemical design of the counterion does not have a marked influence on the optical absorption. The same spectrum shape was obtained applying potentials in the 0.5–0.9 V range, while at a potential below 0.5 V no changes were observed, as expected by the cyclic voltammetry results (Fig. S10). Furthermore, the investigated process shows good reversibility, as evidenced by the quick progressive decrease of the radical cation peaks when moving from a potential of 0.6 V to a negative one of −0.2 V (Fig. S11). To measure the efficiency of the electrochemical production of the radical cation, a previously published procedure[30] was followed, and values of faradaic efficiency (FE) between 13% and 21% were estimated (Table S3). The low FE calculated can be attributed to the deposition of the radical cation within tabular cavities of the honeycomb electrode, which is not consequently optically detected, and to the electrolysis of other species, such as dications. As the potential applied increased, different behaviours were observed. After applying a 0.7 V potential for one minute and producing the previously reported spectrum of the radical cation, a potential of 1.2 V was applied for 100 seconds (Fig. S12). The first 20 seconds of this period showed an increase in the intensity of the radical cation spectrum. However, its peak intensity subsequently declined while the peaks at 668 nm and 740 nm continued to rise. The final spectrum obtained could therefore be attributed to a mixture of the radical cation and the dication, as corroborated by theoretical calculations.

Theoretical calculations

To better understand the absorption features of radical circulenes, we performed density functional theory simulations

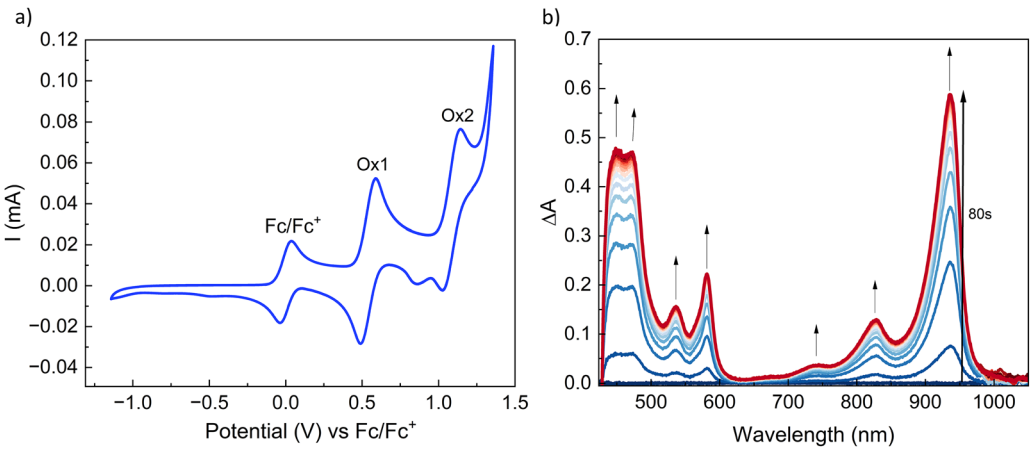

Fig. 4 (a) Cyclic voltammogram of the neutral circulene **C1** recorded in dichloromethane solution (0.1 M $TBAPF_6$) at a scan rate of 100 mV s^{-1} and reported *versus* Fc/Fc^+ couple. Ox1 is the first oxidation potential, Ox2 is the second oxidation potential of the circulene starting material **C1**. (b) Differential absorption spectra of circulene **C1** measured using honeycomb electrode after applying a potential of 0.6 V (*vs.* Fc/Fc^+) for 80 s; spectra were recorded at five-second intervals. The blue line is the spectra recorded at time 0 s and the red one is the spectra recorded after 80 seconds.

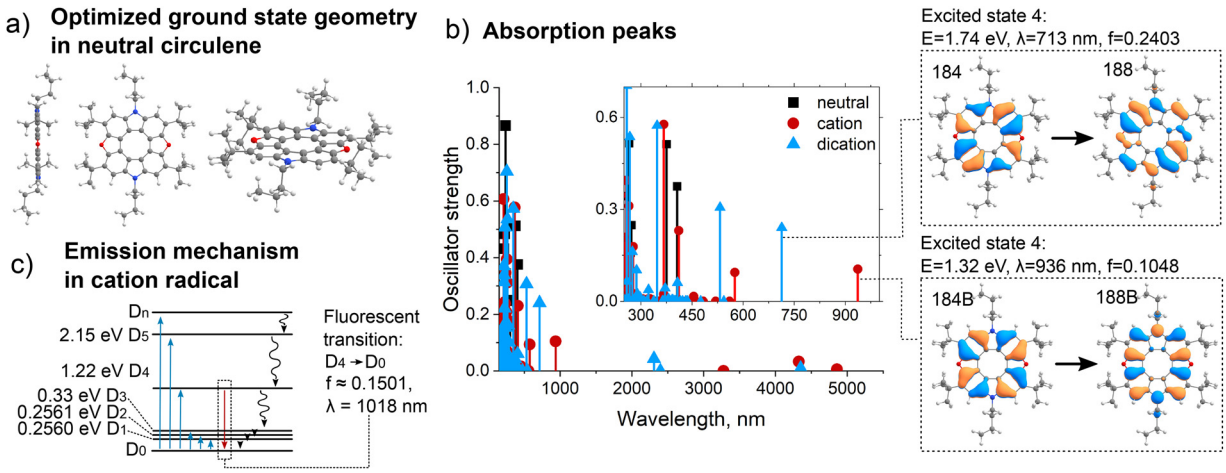

Fig. 5 (a) Optimized geometry of a neutral circulene in its ground state. (b) Simulated absorption peaks of neutral, cationic, and dicationic circulenes (inset shows peaks with $\lambda < 1000$ nm) and visualization of orbitals related to the dominant transitions at 713 nm in dication circulene and at 936 nm in cationic circulene. (c) Calculated emission mechanism through the $D_4 \rightarrow D_0$ transition in cationic circulene.

using the dispersion-corrected GD3BJ-B3LYP[31–33] functional and 6-31+G(d)[34–36] basis set across the whole study. We simulated ground-state geometries (Fig. 5a) and the absorption of neutral, cation, and dication diazadioxa[8]circulenes in the implicit dichloromethane solvent.

Neutral circulene

Despite the optical absorption properties of neutral diazadioxa[8]circulene being well studied, its emission remains unexplained, with ongoing debates in the literature about its origin. While the neutral diazadioxa[8]circulene was experimentally verified as an emitter, time-dependent density functional theory (TD-DFT) indicates that it is supposed to be dark.[37] The $S_1 \rightarrow S_0$ transition, which is expected to be responsible for emission, has a negligible oscillator strength (Table S4). It was proposed that neutral circulene emits through the anti-Kasha $S_2 \rightarrow S_0$ transition,[37] but this explanation can be questioned by the significant energy gap between S_2 and S_1 states. Alternatively, Nakagawa *et al.*[38] proposed that the emission appears "dark" in TD-DFT because the main transitions are symmetry-forbidden, while in experimentally studied systems, Herzberg–Teller vibronic coupling and solvent interactions allow observable emission. Even though the theoretical results were enhanced, this correction was not sufficiently large to provide good agreement with the experiment.[38] In this work, we found that the problem of "dark" S_1 state is related to the artefact of TD-DFT, which flips the energies of the dark state with the emissive state, thus making the emissive state S_2 and the first dark state S_1. This speculation was confirmed by simulations performed with higher levels of theory. Simulation done with RI-CC2 indicates that the $S_1 \rightarrow S_0$ transition occurs at $\lambda = 373$ nm with a large oscillator strength of 0.32, while the $S_2 \rightarrow S_0$ transition occurs at $\lambda = 366$ nm and is effectively "dark" with an oscillator strength of ≈ 0. A similar result was obtained by the ADC (2) method, where the $S_1 \rightarrow S_0$ transition occurs at $\lambda = 379$ nm with a large oscillator strength of 0.34, while the $S_2 \rightarrow S_0$ transition is "dark" with an oscillator strength of ≈ 0. We have performed the RI-CC2/def2-SVP geometry optimization of S_1 and S_2 states and found that the $S_1 \rightarrow S_0$ transition is bright at the S_1 state geometry [2.98 eV and $f = 0.18$] similarly to the $S_1 \rightarrow S_0$ transition at the S_0 geometry [3.32 eV and $f = 0.32$]. Also, we optimized the S_2 state and found that the adiabatic S_2–S_1 gap is 0.1 eV (optimized S_2 is higher than optimized S_1). This confirms that neutral **C1** fluoresces from the S_1 state following the normal Kasha rule in contrast to TD-DFT predictions. Another essential factor, which affects the emission of neutral circulene, is the intersystem crossing. There are four triplet states with energies smaller than the energy of the first singlet excited state (T_1 – 2.16 eV, T_2 – 2.29 eV, T_3 – 2.57 eV, T_4 – 2.59 eV). Specifically, T_4 has similar energy to S_1 (2.74 eV), resulting in a substantial spin–orbit coupling matrix element of 0.6 cm^{-1} and an intersystem crossing (ISC) rate constant of $k_{ISC} = 1.5 \times 10^8\ s^{-1}$. Other triplet T_3, T_2, and T_1 states also contribute to the emission quenching but on a smaller scale with corresponding $k_{ISC}(T_3) = 3.6 \times 10^4\ s^{-1}$, $k_{ISC}(T_2) = 1.2 \times 10^4\ s^{-1}$, $k_{ISC}(T_1) = 2.0 \times 10\ s^{-1}$ (Fig. S17). Following this, we used TD-DFT (MolSOC software) to study photophysics (on S_2 geometry) and obtained a correct quantum yield of $\Phi^{theoretical} = 43\%$ *versus* $\Phi^{experimental} = 30\%$. This quantum yield is primarily determined by intersystem crossing and, to a large extent, by internal conversion processes, as shown in the Jablonski diagram in Fig. S17.

Radical circulene

Withdrawal of one electron changes the electronic structure of the molecule, turning a circulene into a radical with a doublet spin multiplicity. This leads to the appearance of additional low-energy absorption peaks. Three of them are located at $\lambda > 1200$ nm wavelengths (Table S4 and Fig. 5), and some of them even have noticeable oscillator strengths. A new strong peak appears in the NIR at $\lambda = 936$ nm with an oscillator strength of $f \approx 0.1$ (Fig. 5b), which corresponds well with the experimental measurements. This strong absorption peak

predominantly originates from the transition from orbital 184 to LUMO orbital 188 (Fig. 6b) and corresponds to the fourth excited state. Such changes in the electronic structure of the radical compared to neutral circulene are maintained upon further oxidation. Withdrawal of an additional electron eliminates the radical nature of circulene and turns it into a singlet dication. Despite a lack of an unpaired electron, the absorption spectrum of the dication is similar to the cation radical and not to the neutral molecule, with three peaks at large wavelengths $\lambda > 1000$ nm and a strong absorption peak at 713 nm (Table S5).

In most neutral molecules, the emission mechanism follows the Kasha rule and originates from the transition from the lowest excited states showing the same spin of the ground state. However, often in the case of radicals, the emission involves higher excited states and violation of this rule.[39,40] After simulating emission with time-dependent density functional theory, we found that the reported circulene radical should represent the case of anti-Kasha emission. Indeed, because of a very low energy gap of <0.35 eV between the ground state and the first three excited states (Fig. 5c and Table S5), the emission must originate from the fourth excited state $D_4 \rightarrow D_0$ at $\lambda = 1018$ nm. This also allows us to explain the absence of experimentally recorded emission. Several possible quenching pathways involving non-radiative transitions reduce emission intensity to below the detection level. Specifically, there are four internal conversion (IC) pathways for D_4 state dissipation: $D_4 \rightarrow D_0$ ($k_{IC} = 2 \times 10^{10}$ s^{-1}), $D_4 \rightarrow D_1$ ($k_{IC} = 2.5 \times 10^{11}$ s^{-1}), $D_4 \rightarrow D_2$ ($k_{IC} = 2.3 \times 10^{10}$ s^{-1}), and $D_4 \rightarrow D_3$ ($k_{IC} = 9.6 \times 10^{10}$ s^{-1}). By using the Strickler–Berg relation, we can calculate the radiative rate constant $k_r = \frac{1}{1.5} fE^2(D_4 \rightarrow D_0) = 10^7$ s^{-1}.[41] It follows that the resulting quantum yield is $\Phi^{theoretical} = k_r \Big/ \left(k_r + k_{IC}^{D_4 \rightarrow D_0} + k_{IC}^{D_4 \rightarrow D_1} + k_{IC}^{D_4 \rightarrow D_2} + k_{IC}^{D_4 \rightarrow D_3}\right) = 0.025\%$. Such a small quantum yield is a direct consequence of three strong quenching pathways through non-radiative transitions to lower D_3, D_2, and D_1 states (with $D_4 \rightarrow D_1$ IC being the dominant one). Another possible non-radiative quenching channel is the intersystem crossing with quartet states. To exclude this possibility, we simulated the first quartet state and found out that Q_1 is located at a much higher energy (2.12 eV) compared to D_1 (0.26 eV), D_2 (0.29 eV), D_3 (0.38 eV), and even D_4 (1.32 eV). This result confirms the considerable potential of such radical systems in applications that require absorption at the near-infrared part of the spectrum. The possible way to make the **R1** radical fluorescent is to enhance the intensity of the $D_4 \rightarrow D_0$ transition together with shifting it to the blue region. This can be realised by modifying the **C1** core with strong electron-donating groups at the outer perimeter. Another strategy can be the confinement of the radical by the rigid host matrix that helps in suppressing the D_4 non-radiative

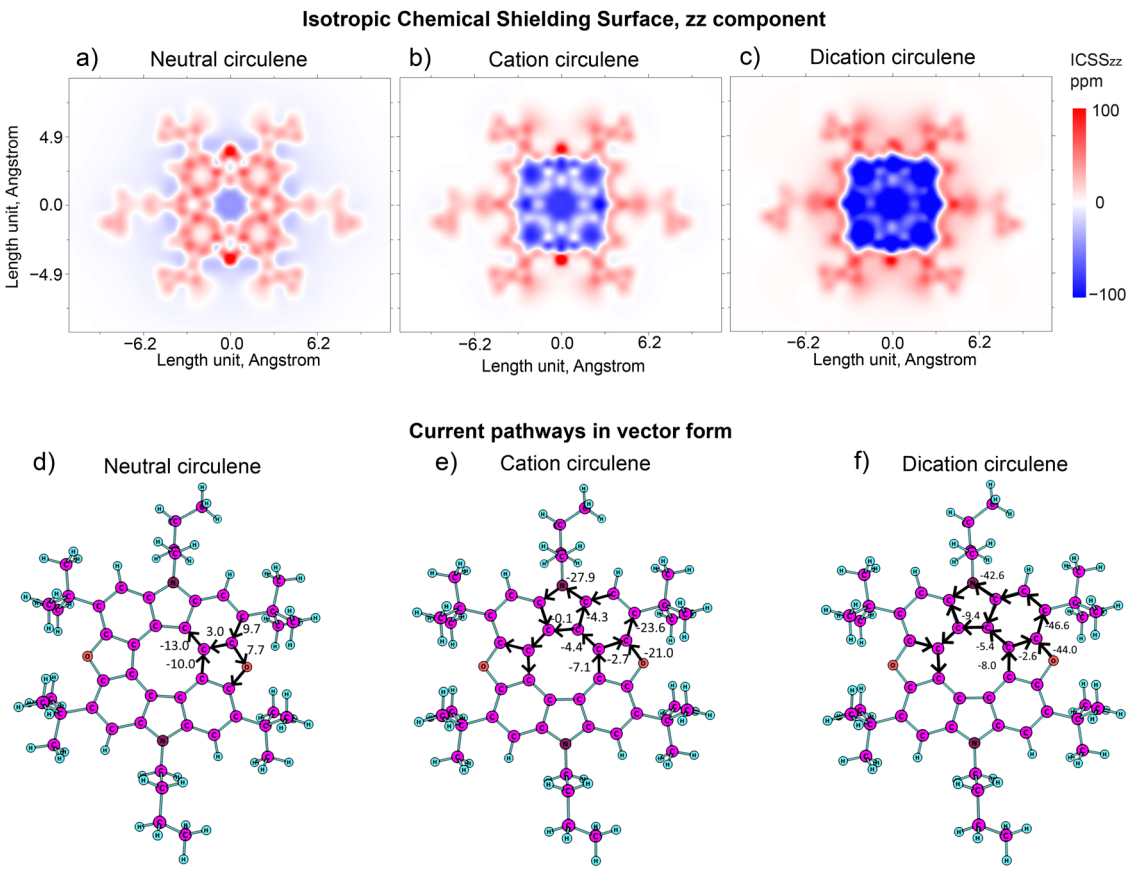

Fig. 6 (a)–(c) $ICSS_{zz}$ depicted in the circulene plane for neutral, cation, and dication molecules. (d)–(f) Current pathways for neutral molecule and its cation and dication counterparts.

quenching into D_3, D_2, D_1, or D_0. Combining the chemical modification with a matrix confinement would have a synergetic effect in achieving $D_4 \rightarrow D_0$ fluorescence.

Aromaticity

[8]Circulenes are polycyclic aromatic hydrocarbons with a central cyclooctatetraene (COT) ring surrounded by eight fused benzene units. Hetero[8]circulenes are analogues, but they have some benzene rings substituted with different heterocycles (thiophene, furan, pyrrole, *etc.*).[42] Neutral hetero[8]circulenes are usually nonaromatic because the paratropic (antiaromatic) current in the COT core cancels out the diatropic (aromatic) current in the outer rim.[43] However, their doubly charged ions (both dications and dianions) often display net diatropic currents, making them globally aromatic, as shown by the results of GIMIC calculations.[43] A similar trend was confirmed by studying another hetero[8]circulenes: neutral molecules are mostly nonaromatic, with some weak antiaromaticity based on substitution.[44] Dianions tend to become aromatic, with strong diatropic currents in both rim and sometimes hub regions. Dications, however, show more varied behaviors—some are aromatic (*e.g.*, SiH- or GeH-based), while others (*e.g.*, O- or NH-containing) are strongly antiaromatic. Overall, the aromaticity of circulenes depends on charge and it is greatly affected by structure and substitution, illustrating how electronic effects influence global delocalization in macrocyclic systems.[44] In the case of diazadioxa[8]circulene, which is the object of this study, we can confirm previous results for its neutral molecules. Visualization of the *zz* component of its isotropic chemical shielding surface ($ICSS_{zz}$) in Fig. 6a shows a paratropic current in the inner ring, compensating for the diatropic current in the outer ring. This is also confirmed by current vectors, depicted in Fig. 6d, where we can clearly see an anti-clockwise paratropic current in the inner ring, a diatropic clockwise vector in the outer ring and a small contribution of the current flowing through radial bonds. Contrary to neutral molecules, electron oxidation makes the molecule anti-aromatic. The cation radical molecule exhibits strong paratropic features in both rings (Fig. 6b). Current vectors depicted in Fig. 6e suggested that current from the inner ring is being interrupted and merges with the current in the outer ring through radical bonds, leading to a global paratropic current (current pathways depicted in Fig. S18). This anti-aromatic behavior can be enhanced by further oxidation of the cation into a dication, resulting in even stronger paratropic current in both inner and outer rings (Fig. 6c and f). In this regard, the aromaticity of radicals represents an intermediate stage between the aromaticity of neutral and dication molecules.

Conclusions

In this work, we report a diazadioxa[8]circulene radical cation exhibiting an intense near-infrared (NIR) absorption at 939 nm. Theoretical simulations predict weak red-shifted radical emission through the anti-Kasha $D_4 \rightarrow D_0$ transition, which is substantially quenched by non-radiative pathways, making it difficult to detect experimentally, and we propose future strategies for achieving $D_4 \rightarrow D_0$ fluorescence.

A key advantage of this platform lies in its synthetic accessibility. The radical cation can be generated in high yield and purity *via* straightforward chemical oxidation with the commercially available one-electron oxidant "Magic Blue." It can also be produced electrochemically under mild conditions, with spectroelectrochemistry confirming that both routes yield the same NIR-active species. The reversible nature of the oxidation and the stability of the radical over days, in both solution and solid-state (at least two days in DCM solution and four days in a PMMA film without significant changes in Vis-NIR absorption spectra), underscore its practical robustness.

The unique combination of strong, tuneable NIR optical response and easy accessibility place diazadioxa[8]circulene radical cations as a promising new class of functional materials. Their stable antiaromatic character further enriches the fundamental understanding of electronically delocalised radicals, while their optoelectronic properties open perspectives for applications in NIR-absorbers, optical sensing, and photonic information technologies. This study thus establishes circulene radical cations as both a novel photophysical phenomenon and an easily deployable materials platform.

Conflicts of interest

The authors declare no conflicts of interest.

Data availability

The data supporting this article have been included as part of the supplementary information (SI). Supplementary information: description of materials and methods, synthesis details, details of FTIR, EPR, UV-Vis, spectroelectrochemistry analysis, stability tests, single-crystal electron diffraction, estimations of faradaic efficiency, and details of theoretical calculations. See DOI: **https://doi.org/10.1039/d6qm00054a**.

CCDC 2494920 (**R1**) contains the supplementary crystallographic data for this paper.[45]

Acknowledgements

The quantum-chemical calculations were performed with computational resources provided by the National Academic Infrastructure for Supercomputing in Sweden (naiss2025-5-140, liu-compute-2025-12, and naiss2024-5-552) at the National Supercomputer Centre (NSC) at Linköping University, partially funded by the Swedish Research Council through grant agreement no. 2022-06725. This work was partially supported by the European Union (ERC, LUMOR, 101077649). G. B. acknowledges the support from the Swedish Research Council through project grant no. 2024-05286 and Swedish Government Strategic Research Area in Materials Science on Advanced Functional Materials at Linköping University (Faculty grant SFO-Mat-LiU

no. 2009-00971). C. B., I. S., M. V., R. K., and G. B. acknowledge the Knut and Alice Wallenberg Foundation (Wallenberg Initiative Materials Science for Sustainability). I. S. and G. B. express gratitude for the support by the ÅForsk (no. 25-316). MP thanks Novonordiskfonden (grant number 0090256) for financial support. Electron diffraction experiments are supported by the Novo Nordisk Foundation Research Infrastructure grant no. NNF220C0074439. The authors acknowledge Prof. Reverant Crispin for the discussions and assistance with the electrochemical part of the manuscript.

References

1 T. Hensel, D. Trpcevski, C. Lind, R. Grosjean, P. Hammershøj, C. B. Nielsen, T. Brock-Nannestad, B. E. Nielsen, M. Schau-Magnussen, B. Minaev, G. V. Baryshnikov, M. Pittelkow, T. Brock-Nannestad, B. E. Nielsen, M. Schau-Magnussen, B. Minaev, G. V. Baryshnikov and M. Pittelkow, Diazadioxa-[8]circulenes: Planar antiaromatic cyclooctatetraenes, *Chem. – Eur. J.*, 2013, **19**, 17097–17102.

2 G. V. Baryshnikov, B. F. Minaev and V. A. Minaeva, Electronic structure, aromaticity and spectra of hetero[8]circulenes, *Russ. Chem. Rev.*, 2015, **84**, 455–484.

3 N. N. Karaush-Karmazin, G. V. Baryshnikov and B. F. Minaev, Aromaticity of Heterocirculenes, *Chem*, 2021, **3**, 1411–1436.

4 K. B. Ivaniuk, G. V. Baryshnikov, P. Y. Stakhira, S. K. Pedersen, M. Pittelkow, A. Lazauskas, D. Volyniuk, J. V. Grazulevicius, B. F. Minaev and H. Ågren, New WOLEDs based on p-extended azatrioxa[8]circulenes, *J. Mater. Chem. C*, 2017, **5**, 4123–4128.

5 S. K. Pedersen, V. B. R. Pedersen, F. S. Kamounah, L. M. Broløs, G. V. Baryshnikov, R. R. Valiev, K. Ivaniuk, P. Stakhira, B. Minaev, N. Karaush-Karmazin, H. Ågren and M. Pittelkow, Dianthracenylazatrioxa[8]circulene: Synthesis, Characterization and Application in OLEDs, *Chem. – Eur. J.*, 2021, **27**, 11609–11617.

6 R. R. Valiev, R. M. Gadirov, K. M. Degtyarenko, D. V. Grigoryev, R. T. Nasubullin, G. V. Baryshnikov, B. F. Minaev, S. K. Pedersen and M. Pittelkow, The blue vibronically resolved electroluminescence of azatrioxa[8]circulene, *Chem. Phys. Lett.*, 2019, **732**, 136667.

7 T. Fujimoto, M. M. Matsushita and K. Awaga, Electrochemical field-effect transistors of octathio[8]circulene robust thin films with ionic liquids, *Chem. Phys. Lett.*, 2009, **483**, 81–83.

8 A. Dadvand, F. Cicoira, K. Y. Chernichenko, E. S. Balenkova, R. M. Osuna, F. Rosei, V. G. Nenajdenko and D. F. Perepichka, Heterocirculenes as a new class of organic semiconductors, *Chem. Commun.*, 2008, 5354–5356.

9 T. Fujimoto, M. M. Matsushita and K. Awaga, Dual-gate field-effect transistors of octathio[8]circulene thin-films with ionic liquid and SiO2 gate dielectrics, *Appl. Phys. Lett.*, 2010, **97**, 2008–2011.

10 Z. Chang, M. Zhu, Z. Li, S. Wu, S. Yin, Y. Sun and W. Xu, 2D Conductive Metal-Organic Frameworks Based on Tetraoxa[8]-circulenes as Promising Cathode for Aqueous Zinc Ion Batteries, *Small*, 2024, **20**, 1–9.

11 Z. Chang, M. Zhu, Y. Sun, F. He, Y. Li, C. Ye, Y. Jin, Z. Li and W. Xu, A Conductive 2D Conjugated Tetrathia[8]circulene-Based Nickel Metal–Organic Framework for Energy Storage, *Adv. Funct. Mater.*, 2023, **33**, 1–7.

12 P. W. Fritz, T. Chen, T. Ashirov, A. D. Nguyen, M. Dincă and A. Coskun, Fully Conjugated Tetraoxa[8]circulene-Based Porous Semiconducting Polymers, *Angew. Chem., Int. Ed.*, 2022, **61**, e202116527.

13 Q. Chen, M. Baumgarten, M. Wagner, Y. Hu, I. C. Hou, A. Narita and K. Müllen, Dicyclopentaannelated Hexa- peri -hexabenzocoronenes with a Singlet Biradical Ground State, *Angew. Chem., Int. Ed.*, 2021, **60**, 11300–11304.

14 L. Yuan, J. Yang, S. Qi, Y. Liu, X. Tian, T. Jia, Y. Wang and C. Dou, Diradicaloid Boron-Doped Molecular Carbons Achieved by Pentagon-Fusion, *Angew. Chem., Int. Ed.*, 2023, **62**, e202314982.

15 Y. Hamamoto, W. Wang, Y. Li and S. Ito, Azadihomocoranulene as a Heptagon-Embedded Diradicaloid, *Angew. Chem., Int. Ed.*, 2025, **64**, e202416654.

16 Y. Zou, L. Jiao, Y. Han, L. Ren, Q. Zhou and J. Wu, Peri -pentacene and Peri -hexacene Diradicaloids, *J. Am. Chem. Soc.*, 2024, **146**, 27293–27298.

17 L. Yuan, S. Qi, P. Lv, T. Jia, Z. Fan, X. Tian, N. Guan and C. Dou, Acenaphthylene-Fusion Enabling Stable Organic Diradicaloids with Large Singlet–Triplet Energy Gap for Photothermal Utility, *CCS Chem.*, 2026, **8**, 1001–1010.

18 M. Imran, C. M. Wehrmann and M. S. Chen, Open-Shell Effects on Optoelectronic Properties: Antiambipolar Charge Transport and Anti-Kasha Doublet Emission from a N-Substituted Bisphenalenyl, *J. Am. Chem. Soc.*, 2020, **142**, 38–43.

19 C. M. Wehrmann, M. Imran, C. Pointer, L. A. Fredin, E. R. Young and M. S. Chen, Spin multiplicity effects in doublet: Versus singlet emission: The photophysical consequences of a single electron, *Chem. Sci.*, 2020, **11**, 10212–10219.

20 M. Ito, S. Shirai, Y. Xie, T. Kushida, N. Ando, H. Soutome, K. J. Fujimoto, T. Yanai, K. Tabata, Y. Miyata, H. Kita and S. Yamaguchi, Fluorescent Organic π-Radicals Stabilized with Boron: Featuring a SOMO–LUMO Electronic Transition, *Angew. Chem., Int. Ed.*, 2022, **61**, e202201965.

21 J. Jin, W. Chen, J. Tan, Y. Li, Y. Mu, Z. Zhu, C. Cao, S. Ji, D. Hu, Y. Huo, H. Zhang and C. Lee, Photo-controllable Luminescence from Radicals Leading to Ratiometric Emission Switching via Dynamic Intermolecular Coupling, *Angew. Chem., Int. Ed.*, 2023, **62**, e202214281.

22 R. Rathore and S. H. Abdelwahed, Soluble cycloannulated tetroxa[8]circulane derivatives: Synthesis, optical and electrochemical properties, and generation of their robust cation–radical salts, *Tetrahedron Lett.*, 2004, **45**, 5267–5270.

23 Y. Matsuo, T. Tanaka and A. Osuka, Highly Stable Radical Cations of N,N′-Diarylated Tetrabenzotetraaza[8]circulene, *Chem. – Eur. J.*, 2020, **26**, 8144–8152.

24 A. I. Hofmann, R. Kroon, S. Zokaei, E. Järsvall, C. Malacrida, S. Ludwigs, T. Biskup and C. Müller, Chemical Doping of Conjugated Polymers with the Strong Oxidant Magic Blue, *Adv. Electron. Mater.*, 2020, **6**, 1–8.

25 S. Zhang, H. M. Hill, K. Moudgil, C. A. Richter, A. R. Hight Walker, S. Barlow, S. R. Marder, C. A. Hacker and S. J. Pookpanratana, Controllable, Wide-Ranging n-Doping and p-Doping of Monolayer Group 6 Transition-Metal Disulfides and Diselenides, *Adv. Mater.*, 2018, **30**, 1802991.
26 V. A. Minaeva, B. F. Minaev, G. V. Baryshnikov and M. Pittelkow, Raman spectra of alkyl-substituted azaoxa[8]circulenes: DFT calculation and experiment, *Opt. Spectrosc.*, 2013, **114**, 509–521.
27 Y. Matsuo, T. Tanaka and A. Osuka, Diazadimethano[8]-circulene: Synthesis, structure, properties, and isolation of stable radical cation, *Chem. Lett.*, 2020, **49**, 959–962.
28 L. Petrakis, Spectral Line Shapes. Gaussian and Lorentzian functions in magnetic resonance, *J. Chem. Educ.*, 1967, **44**, 432–436.
29 N. G. Connelly and W. E. Geiger, Chemical redox agents for organometallic chemistry, *Chem. Rev.*, 1996, **96**, 877–910.
30 H. G. Shiraz, M. Vagin, T. P. Ruoko, V. Gueskine, K. Karoń, M. Łapkowski, T. Abrahamsson, T. Ederth, M. Berggren and X. Crispin, Towards electrochemical hydrogen storage in liquid organic hydrogen carriers *via* proton-coupled electron transfers, *J. Energy Chem.*, 2022, **73**, 292–300.
31 S. Grimme, S. Ehrlich and L. Goerigk, Effect of the damping function in dispersion corrected density functional theory, *J. Comput. Chem.*, 2011, **32**, 1456–1465.
32 A. D. Becke and E. R. Johnson, A density-functional model of the dispersion interaction, *J. Chem. Phys.*, 2005, **123**, 154101.
33 C. Lee, W. Yang and R. G. Parr, Development of the Colic-Salvetti correlation-energy formula into a functional of the electron density, *Phys. Rev. B:Condens. Matter Mater. Phys.*, 1988, **37**, 785–789.
34 R. Ditchfield, W. J. Hehre and J. A. Pople, Self-Consistent Molecular-Orbital Methods. IX. An Extended Gaussian-Type Basis for Molecular-Orbital Studies of Organic Molecules, *J. Chem. Phys.*, 1971, **54**, 724–728.
35 T. Clark, J. Chandrasekhar, G. W. Spitznagel and P. V. R. Schleyer, Efficient diffuse function-augmented basis sets for anion calculations. III. The 3-21+G basis set for first-row elements, Li–F, *J. Comput. Chem.*, 1983, **4**, 294–301.
36 M. J. Frisch, J. A. Pople and J. S. Binkley, Self-consistent molecular orbital methods 25. Supplementary functions for Gaussian basis sets, *J. Chem. Phys.*, 1984, **80**, 3265–3269.
37 G. V. Baryshnikov, R. R. Valiev, N. N. Karaush, V. A. Minaeva, A. N. Sinelnikov, S. K. Pedersen, M. Pittelkow, B. F. Minaev and H. Ågren, Benzoannelated aza-, oxa- and azaoxa[8]circulenes as promising blue organic emitters, *Phys. Chem. Chem. Phys.*, 2016, **18**, 28040–28051.
38 A. Nakagawa, W. Ota, T. Ehara, Y. Matsuo, K. Miyata, K. Onda, T. Sato, S. Seki and T. Tanaka, Synthesis of substituent-free dioxadiaza[8]circulene to investigate intermolecular interactions and photophysical properties, *Chem. Commun.*, 2024, **60**, 14770–14773.
39 Y. Li, G. V. Baryshnikov, C. Xu, H. Ågren, L. Zhu, T. Yi, Y. Zhao and H. Wu, Photoinduced Radical Emission in a Coassembly System, *Angew. Chem., Int. Ed.*, 2021, **60**, 23842–23848.
40 I. Sahalianov, R. R. Valiev, R. R. Ramazanov and G. Baryshnikov, Neutral vs Charged Luminescent Radicals: Anti-Kasha Emission and the Impact of Molecular Surrounding, *J. Phys. Chem. A*, 2024, **128**, 5138–5145.
41 S. J. Strickler and R. A. Berg, Relationship between absorption intensity and fluorescence lifetime of molecules, *J. Chem. Phys.*, 1962, **37**, 814–822.
42 Y. Miyake and H. Shinokubo, Hetero[8]Circulenes: Synthetic Progress and Intrinsic Properties, *Chem. Commun.*, 2020, **56**, 15605–15614.
43 G. V. Baryshnikov, R. R. Valiev, N. N. Karaush and B. F. Minaev, Aromaticity of the planar hetero[8]circulenes and their doubly charged ions: NICS and GIMIC characterization†, *Phys. Chem. Chem. Phys.*, 2014, **16**, 15367–15374.
44 G. V. Baryshnikov, R. R. Valiev, N. N. Karaush, D. Sundholm and B. F. Minaev, Aromaticity of the doubly charged [8]circulenes, *Phys. Chem. Chem. Phys.*, 2016, **18**, 8980–8992.
45 CCDC 2494920: Experimental Crystal Structure Determination, 2026, DOI: **10.5517/ccdc.csd.cc2pr59y**.